energy&fuels

pubs.acs.org/EF

Article

Wireless Electrochemically Driven Combustion of Ionic Liquid Fuel

Afrida Anis, Keren Shi, Erik Hagen, and Michael R. Zachariah*

Cite This: *Energy Fuels* 2026, 40, 17838−17847

Read Online

ACCESS | Metrics & More | Article Recommendations | Supporting Information

ABSTRACT: The flammability and combustion behavior of liquid fuels are primarily governed by volatility, often causing unintended ignition. Room temperature ionic liquids (RTILs) are generally considered nonflammable due to negligible vapor pressure and superior thermal stability. These nonvolatile RTILs can be rendered electrochemically combustible enabling a safer fuel concept with on-demand flame extinction. This work introduces bipolar electrochemistry as a wireless strategy to enhance the kinetics of electrochemically combustible RTIL fuels. Under an applied electric field, polarization of the bipolar electrode drives simultaneous oxidation and reduction reactions without direct electrical wiring. The effects of BPE materials and characteristic dimensions are investigated using electrochemical measurements and compared against a no-BPE system. Carbon foam BPEs exhibit superior performance, achieving up to a 4-fold reactivity enhancement compared to the no-BPE configuration. Correspondingly, electrochemical combustion power generation enhances by a factor of ∼4.5. A developed model incorporating the specific operating conditions predicts a 2.3-fold enhancement arising from the additional reactive surface area under isothermal conditions. Under nonisothermal conditions, ionic Joule heating increases conductivity yielding a combined enhancement of up to 6.9-fold. These findings highlight bipolar electrochemistry as a controllable, hardware-efficient strategy in regulating the electrochemical combustion performance of ionic liquid fuels.

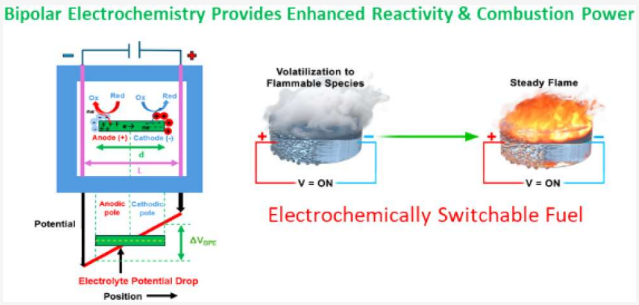

1. INTRODUCTION

High-energy-density liquid fuels burn in the gas phase, and their flammability is strongly tied to their vapor pressure.[1,2] This typically necessitates safety concerns, resulting from the possibility of unintended ignition and potentially requiring specialized storage. Condensed-state fuels achieve self-sustained combustion through heat feedback from the flame, sufficient to vaporize and ignite the fuel under steady-state conditions.[1−3] The usual strategy to extinguish the flame is the removal of air.

Another strategy we may consider is to dynamically manipulate the volatility of the fuel by an electrochemical switch. We are particularly interested in a special class of compounds, room temperature ionic liquids (RTILs), defined as salts with melting points below 100 °C and extremely low vapor pressure at room temperature.[4−12] However, RTILs also possess high energy densities which make them attractive fuel candidates for propulsion.[13] For example, compounds classified as Energetic ionic liquids (EILs), consisting of metastable anions such as azide, dinitramide, borohydride, and azole-based anions, are known to thermally decompose into reactive flammable species.[14−18] This has led to the use of such RTILs as fuel components in propellant and explosive formulations. Additionally, thermally insensitive RTILs without such reactive anions can also be chemically activated with white fuming nitric acid enabling them to oxidize spontaneously resulting in hypergolic ignition.[12,14] Extinction of the flame is difficult in such cases since they need the separation of the fuel and oxidizer components.

Recently, electrically controlled solid propellants (ECSP) and gel propellants (ECGP) have gained much attention as they can be manipulated through electrical means to control ignition and throttling burn rates.[19] Several studies on ECSPs have found that to manipulate the combustion velocity, the creation of a liquid melt layer is needed through ohmic heating leading to the thermal decomposition of the ECSP constituents or electrochemical decomposition upon the application of an electrical load that can exceed 100 V.[19−21] This is an indication of the liquid being much more easily manipulated as it can facilitate thermal or electrochemical decomposition at a lower applied load than the ECSPs because ions have higher mobility through liquid than solid.

In our group's previous works, we have demonstrated that we can dynamically manipulate the volatility of the nominally involatile and thermally stable RTILs through electrochemical means, making nonflammable RTILs flammable.[22,23] Via in-operando mass spectrometry, we found that the aromaticity of

Received: April 30, 2026
Revised: July 28, 2026
Accepted: July 29, 2026
Published: August 4, 2026

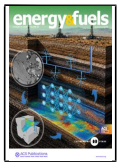

https://doi.org/10.1021/acs.energyfuels.6c02293
Energy Fuels 2026, 40, 17838−17847

the imidazole ring cations of the apparently thermally stable and nonflammable imidazole-based RTILs can be broken electrochemically resulting in their volatilization as reactive flammable species which can be ignited to create a stable flame (Figure 1b–c). Additionally, we demonstrated that the

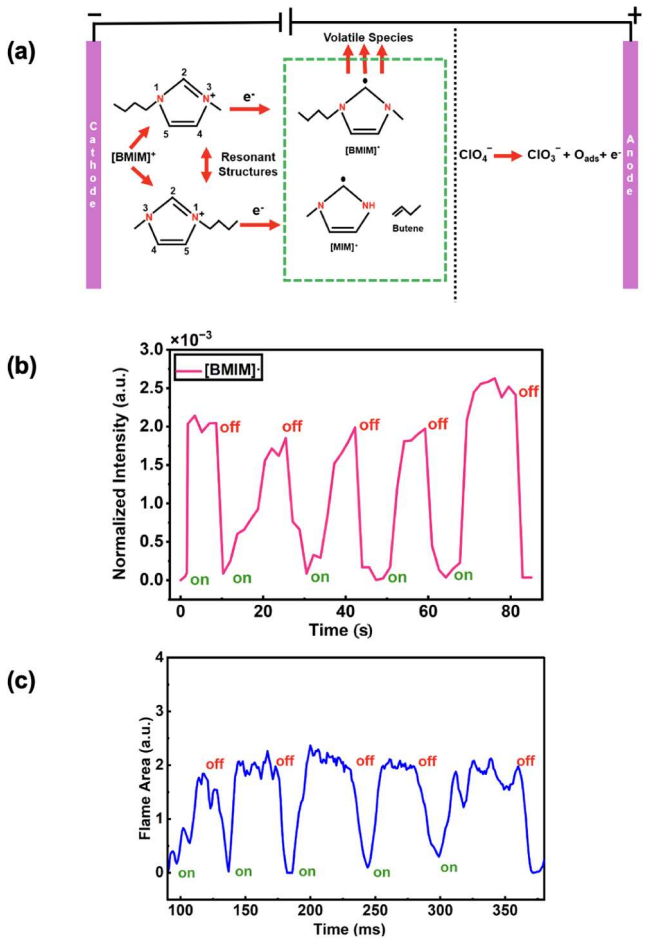

Figure 1. (a) Electrochemical decomposition mechanism of $[BMIM]^+[ClO_4]^-$ RTIL. (b) Sequential volatilization of $[BMIM]^+[ClO_4]^-$ as flammable $[BMIM]^\bullet$. (c) Flame area as a function of time during the electrochemical combustion of $[BMIM]^+[ClO_4]^-$ captured from high-speed camera imaging.

removal of the applied voltage bias terminates the electrochemical reactions, thereby stopping the volatilization of the RTILs and resulting in the extinction of the flame (Figure 1b–c). This process can be repeated to undergo ignition–extinction as a tool to control or throttle the process. As the RTIL is thermally insensitive, the heat feedback from the flame is unable to generate significant vapor pressure or flammable gas-phase species from the fuel. Hence, it can only ignite the flammable vapor-phase species generated electrochemically and is unable to ignite the liquid RTIL thermally. Figure 1a shows the proposed electrochemical decomposition mechanism, as determined by in situ mass spectrometry, Figure 1b demonstrates the sequential volatilization of the model RTIL, 1-butyl-3-methyl imidazolium perchlorate ($[BMIM]^+[ClO_4]^-$) during in-operando mass spectrometry as flammable $[BMIM]^\bullet$ and Figure 1c demonstrates the flame area measured during the electrochemically controlled combustion by high-speed imaging.[22,23]

In our previous studies, we determined that the overall electrochemical rate and thus the combustion intensity of RTILs in our system is limited by ion transport from the bulk to the electrode surfaces.[22] To amplify the kinetics of combustible species generation electrochemically, in this work, we explore a relatively new development called "bipolar electrochemistry" for driving electrochemical reactions wirelessly.[24] This approach relies on the wireless nature of the bipolar electrodes leveraging electric field-induced polarization of the conductor immersed in the electrolyte solution to drive cathodic and anodic reactions simultaneously at spatially distinct poles making it of great interest in sensor development and material synthesis.[25−27] The basic concept is illustrated in Figure 2a. In conventional electrode configurations, steep potential gradients exist at the electrical double layer, which drive the redox reactions. For simplicity of analysis, here we assume that for the system with a conductive bipolar electrode (BPE) immersed in the electrolyte, most of the potential drop happens in the bulk of the electrolyte (RTIL in this work) neglecting the EDL effect at the driving electrode/electrolyte interface since the gap between the driving electrodes is much larger in scale.[28] The lateral drop in potential in the RTIL results in the potential of the immersed BPE floating to an equilibrium potential, V_{elec}, that separates the BPE into two poles, the cathodic pole where the RTIL potential is higher than V_{elec} and the anodic pole where the RTIL potential is lower than V_{elec}. Accordingly, there is a potential difference at each lateral position of the RTIL/electrode interface that may or may not drive the redox reactions at the poles of the corresponding BPE. To drive an electrochemical reaction, the potential difference at the two ends of the BPE, ΔV_{BPE}, must be higher than the stability window of the RTIL.[27] The potential difference at the bipolar electrode/RTIL interface is governed by the electric field established within the RTIL.[29] Local regions with large interfacial potential differences have higher local driving force for electron transfer and ion transport than the uniform field resulting in an overall improved reaction kinetics for a BPE system.[30,31] Leveraging the wireless nature of the bipolar electrode, we demonstrate, for the first time, significantly improved reaction kinetics and combustion power generation for electrochemically combustible RTIL fuel with just two driving electrodes and one power supply, an achievement that has not been realized before in the domain of condensed-phase propellants.

2. EXPERIMENTAL SECTION

2.1. RTIL Preparation

For these demonstrations, we used $[BMIM]^+[ClO_4]^-$ as our RTIL fuel following our previous studies.[22,23] We prepared the RTIL by an ion exchange method between $[BMIM]^+[Cl]^-$ and $NaClO_4$. $[BMIM]^+[Cl]^-$ (~98%) solid powder (mp ~ 70 °C) was procured from Sigma-Aldrich. Anhydrous $NaClO_4$ crystals, ACS, 98–102%, were bought from Thermo Scientific. More details on the synthesis of $[BMIM]^+[ClO_4]^-$ can be found in the Supporting Section S1.

2.2. BPE Materials

All the bipolar electrodes used in this study were rectangular in shape with a fixed length of 12 mm and a varying width of 5–9 mm to investigate the impact of the distance between driving electrodes and the electrochemically active poles of the BPE on the electrochemical reactivity of the RTIL fuel. For BPE materials, we chose carbon and nickel foams, and sputter-deposited platinum on a thin glass substrate. Among these electrode materials, carbon and nickel foams were chosen owing to their high specific surface area, porosity, and porous

https://doi.org/10.1021/acs.energyfuels.6c02293
Energy Fuels 2026, 40, 17838−17847

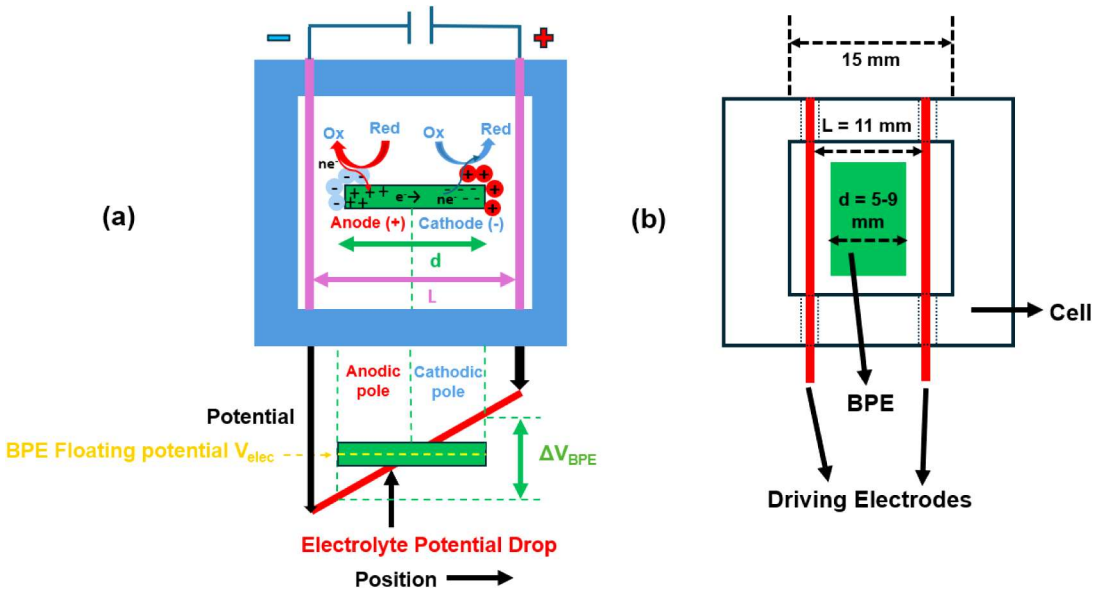

Figure 2. (a) Schematic of bipolar electrochemistry. (b) Schematic of an electrochemical cell with a BPE (shown in green).

conductive network for better electron and ion transfer capability.[32−34] The carbon foam was procured from Zopin Group, China, and the nickel foam was bought from MSE Supplies LLC, United States. Pt-deposited BPEs were fabricated by physical vapor deposition using a magnetron sputtering system (ORION 5, AJA) on cover glasses (Thermo Scientific). Photolithographic patterning was performed prior to metal deposition. Approximately 15 nm of Titanium was deposited as an adhesive layer, followed by approximately 100 nm of Platinum. The total thickness of the bipolar electrodes was 115 ± 6 nm as measured by a profilometer (Dektak 8, Veeco).

2.3. Electrochemical Measurements

For the electrochemical studies, we fabricated a cell using VeroUltra WhiteS resin with dimensions of 25 mm × 25 mm × 3 mm. A schematic of the cell with the BPE inside is shown in Figure 2b. The cell has through-holes for inserting the platinum driving electrodes (diameter: 75 μm) and has copper supports for attaching the platinum wire electrodes so that they remain fixed. The platinum electrodes were connected to the power source to apply the DC voltage bias. The distance between the driving electrodes was fixed at 11 mm. A Bipolar electrode of specific dimensions was placed between the driving electrodes, and by changing the width of the BPE, we could vary the distance between the driving electrodes and the bipolar electrode. Figure 3 provides evidence that the BPE is in fact active as gas bubble formation at the induced cathodic pole of the BPE is clearly observed. Current was measured using a Hewlett-Packard 34401A digital multimeter, and for the linear sweep voltammetry measurements, we used an AMEL 2553 high-voltage potentiostat-galvanostat.

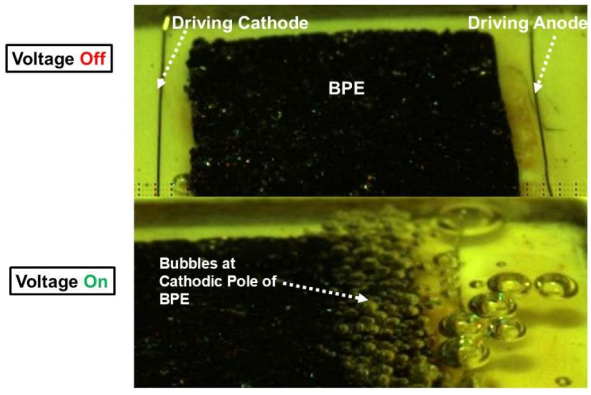

Figure 3. Gas generation as evidence of bipolar electrode's activity during electrolysis.

2.4. Linear Sweep Voltammetry

To determine the stable voltage region where no electrochemical reaction occurs for the RTIL fuel, we used linear sweep voltammetry (LSV). LSV provides the threshold voltage necessary to induce electrochemical reactions as indicated by the sharp current onset in the I−V polarization curve.[35] By calculating the difference between the onset potentials of oxidation and reduction reactions, we can determine the minimum applied voltage required for RTIL decomposition.

2.5. Electrochemical Combustion Switchability of RTIL Fuel

For demonstrating electrochemically controlled combustion, 1.5 mmol of RTIL fuel was placed in the cavity of the fabricated electrochemical cell shown in Figure 2b. Without electrochemical activation, when the RTIL was exposed to a butane torch (ignition source), no ignition was observed indicating $[BMIM]^+[ClO_4]^-$ is nonflammable thermally. However, when sufficient voltage (beyond stable region determined from LSV) was applied to drive the electrochemical reaction, significant bubble formation and gas generation were observed. A steady flame can be generated, and its area can be measured as shown in Figure 1c. Upon voltage removal, the flame will be extinguished, and this can be repeated as required. The combustion event was captured with a Phantom Miro M110 high-speed color camera with a Nikon 105 mm f/2.8 AF micro lens. For flame area calculation (Figure 1c), the images were binarized to isolate the flame in the image. The bright pixels were counted and multiplied by the area of each pixel to get the flame area.

2.6. Temperature Measurement by IR Imaging

The measurement of the temporal and spatial distribution of surface temperature of the RTIL fuel during the electrochemical decomposition was measured with a Telops FAST M3K IR camera. The videos were recorded with a 50 mm lens and a 0.5-in. extension ring using a 10 μs exposure time, at 100 Hz and a resolution of 105 μm per pixel. The emissivity of the ionic liquid was assumed to be 1 and independent of temperature.

https://doi.org/10.1021/acs.energyfuels.6c02293
Energy Fuels 2026, 40, 17838−17847

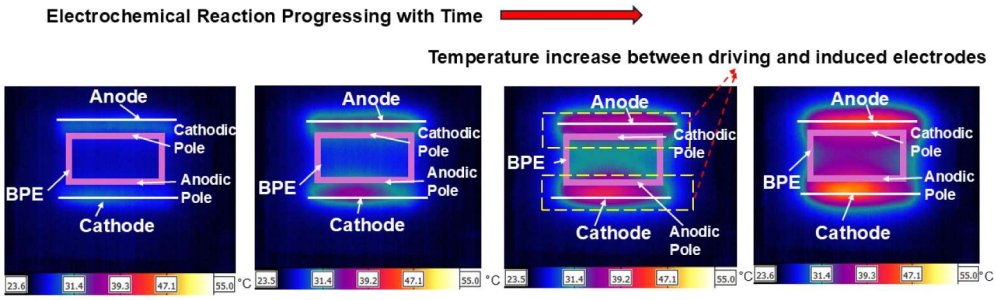

Figure 4. Temporal IR thermograph of a BPE system during electrolysis.

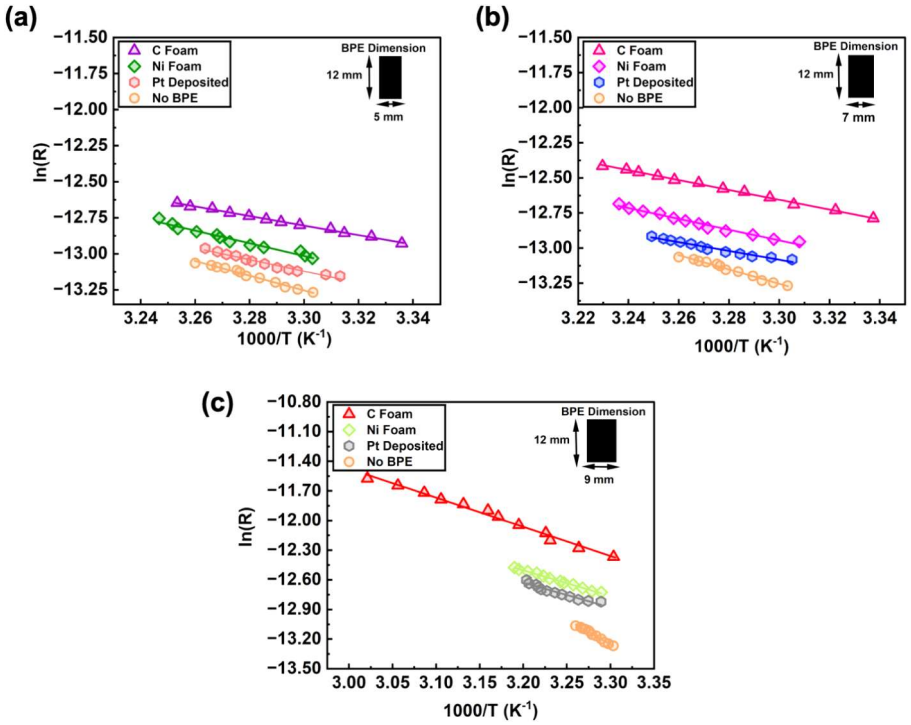

Figure 5. Arrhenius plots of electrochemical reaction rates for BPE and no-BPE systems at 25 V for BPE dimensions of (a) 12 mm × 5 mm, (b) 12 mm × 7 mm, and (c) 12 mm × 9 mm.

3. RESULTS AND DISCUSSIONS

3.1. Electrochemical Reactivity Comparison

Figure 1a outlines the proposed decomposition mechanism of RTIL fuel $[BMIM]^+[ClO_4]^-$ to generate volatile reactive species at the cathode (in the BPE system, both at the driving cathode and the induced cathodic pole of the bipolar electrode).[23] Our previous study demonstrated that our electrochemical system is not strictly isothermal owing to ionic Joule heating in the RTIL.[22] Thermal imaging using an IR camera of the RTIL, with an immersed BPE, further confirms Joule heating as shown in Figure 4. The reported instantaneous temperatures were averaged over the entire RTIL solution for both BPE and no-BPE systems, and this allows us to plot the measured reaction rate as a function of temperature as demonstrated in Figure 5. In this study, the electrochemical rate measurements for all BPEs were done at 25 V, which is higher than the stable voltage window of this RTIL.[22] In Figure 5, we show Arrhenius plots of the rate during electrolysis for all BPE materials at three different dimensional configurations and compare their rates with a no-BPE system. In our experiments, we measure the current, and with a known surface area of the driving electrode, we convert it to current density. The relationship between reaction rate, R, and current density can be written as follows:

$$R = \frac{J}{F} \tag{1}$$

where R is the is the surface reaction rate expressed in moles cm^{-2} s^{-1}, J is the current density expressed in amperes (A)·cm^{-2}, and F is the Faraday's constant for a one electron transfer process.[36]

As noted earlier, all bipolar electrodes (BPEs) in this study had a fixed length of 12 mm to ensure a perfect fit within the cell. The BPE width, d, in Figure 2b was varied from 5 to 9 mm to systematically investigate the effect of the distance between driving electrodes and the BPE while keeping the separation between the driving electrodes constant. From Figure 5, we can observe that the reaction rate increases with temperature and that for all dimensions of BPEs the reaction rate is in the order:

C foam > Ni foam > Deposited Pt > no BPE

https://doi.org/10.1021/acs.energyfuels.6c02293
Energy Fuels 2026, 40, 17838−17847

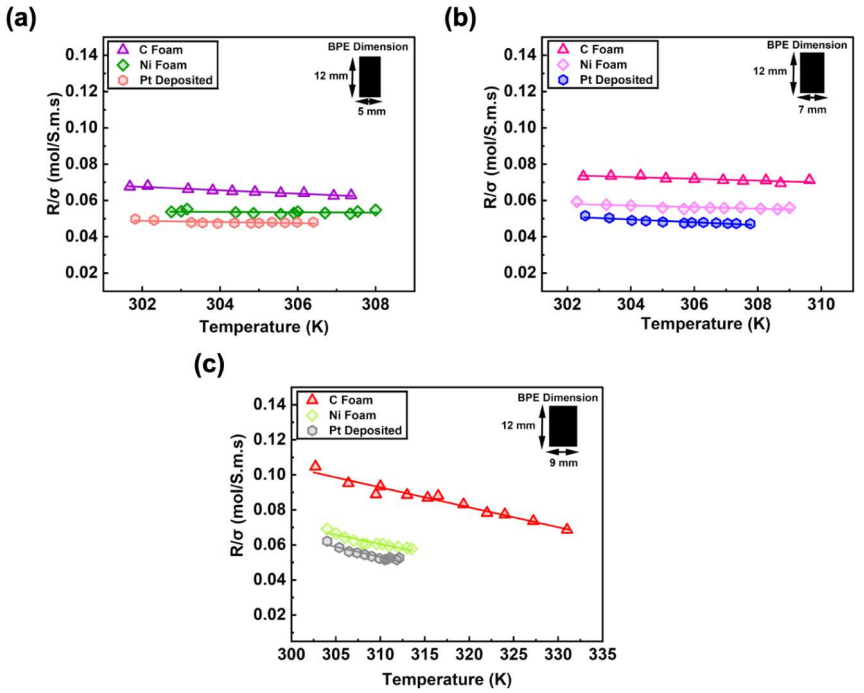

Figure 6. Normalized electrochemical reaction rates comparison between BPE and no-BPE systems at 25 V for BPE dimensions of (a) 12 mm × 5 mm, (b) 12 mm × 7 mm, and (c) 12 mm × 9 mm.

As a BPE material, carbon foam (C foam) outperforms all other BPE materials and the no-BPE system. The factors that affect the surface reaction rate can be classified into four general categories: external variables (pressure, time), electrical variables (potential, charge), electrolyte variables (temperature, conductivity, flow velocity, bulk concentration), and electrode variables (material, geometry).[37] The impact of external variables, including the driving electrode's material and geometry, are being neglected here since those conditions remain unchanged for the BPE and no-BPE systems. As shown earlier in Figure 2a, in a BPE system the electric field across the electrolyte (RTIL) induces polarization at the two edges of the immersed conductor (BPE) driving both cathodic and anodic reactions simultaneously besides the driving electrodes.[25−27] Since the faradaic reactions occur at the two extremes of the conductive BPE, they consume/generate ions creating steep concentration gradients at the poles which in turn create electric field gradients at the BPE/RTIL interface driving more ions toward the BPE surface.[30,38] Our previous study demonstrated that our electrochemical system is strongly mass transport-limited, primarily due to the strong intermolecular interactions in the RTILs which adversely affect their transport properties and ultimately become the limiting factor.[22] Since a BPE system can sustain simultaneous faradaic reactions in addition to the driving electrodes, it provides more active redox sites and can improve ion migration by creating large potential gradients near the BPE/solution interface. Together, these effects can lead to improved reaction kinetics for the RTIL system compared to the no-BPE system as observed in Figure 5.[29,30,30,31,38]

The superior performance of foam materials compared to Pt metal deposited on a glass substrate when used as BPEs can be attributed to the high specific surface area for redox reactions as reported in several literature sources.[32−34,39] In addition, the tortuous three-dimensional network of the foam can provide enhanced contact with the RTIL enabling more effective electrochemical activity than the thin Pt film.[32−34] As evident from Figure 5 compared to C foam, Ni foam did not improve the reactivity as much despite having high specific surface area and conductivity. However, unlike carbon, nickel is not as inert electrochemically and can undergo corrosion and passivation due to its own redox activity which ultimately may degrade its performance as an electrode material.[39,40] Owing to the structural complexity of the foam, definitive conclusions cannot be drawn at this stage.

Figure 5a compares the electrochemical species generation rates for systems with and without a BPE where the BPE width is 5 mm. For this dimension of the BPE, we see that the C foam has a higher rate, by a factor of ∼1.5 relative to the no-BPE system. As we increase the width of the BPE to 7 mm, in Figure 5b we observe an increase in the rate for the C foam BPE compared to the no-BPE system by a factor of ∼2, and subsequently by a factor of ∼4 when we further increase the width to 9 mm in Figure 5c. In all cases, the slopes of the reaction rate as a function of temperature are effectively independent of material type or even if a BPE is used. This implies that the electrochemical mechanism is independent of BPE use or the material type of BPE.

There are, however, a few questions we wish to address in the subsequent sections: does the incorporation of BPE change the rate-limiting step compared to the no-BPE system? What is the role of BPE characteristic dimension or, in other words, the separation distance between the driving electrode and the induced BPE pole on the reaction efficiency?

From our previous study, we concluded that the spatially homogeneous nature of the temperature rise observed through IR imaging during electrolysis implies it is not related to any exothermicity at the electrode but rather should be attributed to dissipative Joule heating and thus related to ion transport.[22] We already argued that the reactivity improvement we observed for the BPE systems compared to the no-BPE system (Figure 5) is possibly due to potential/electric field

https://doi.org/10.1021/acs.energyfuels.6c02293
Energy Fuels 2026, 40, 17838−17847

gradient-induced improved ion transport toward the poles of BPEs. The localized Joule heating in Figure 4 further supports our argument of ion transport between the driving electrodes and the poles of the BPE. Furthermore, we extend our study to explore this point through an assessment of the temperature dependence of ion transport, i.e., ion conductivity, through the Vogel–Fulcher–Tammann (VFT) correlation, following our previous study:[22]

$$\sigma(T) = \sigma_o \exp\frac{-A}{(T - T_{o,\sigma})} \quad (2)$$

where σ is the conductivity and σ_o, A, and $T_{o,\sigma}$ are fitting parameters.

To assess if the Arrhenius behavior observed in Figure 5 can be attributed to reaction kinetics or transport, we normalize the experimental reaction rates by the estimated temperature-dependent conductivity (eq 2) as shown in Figure 6(a–c). The parameters used for conductivity estimation using the VFT correlation can be found in the Supporting Section S2. Figure 6(a–c) shows that for all BPE materials, the reaction rate R normalized by conductivity σ remains mostly constant over the entire temperature range indicating that the Arrhenius behavior can be directly attributed to an increase in ion conductivity. Furthermore, this rate-limiting process is true for both the BPE and no-BPE systems reported previously.[22]

All the data show a slight decrease in reaction rate at least for C foam BPEs, which we attribute to the gradual depletion of reactant, since the higher temperature measurements are obtained at later times. The 9 mm (Figure 6c) BPE shows the most pronounced effects since it has the highest reaction rate, and thus the effects of reactant depletion are more pronounced.

3.2. Influence of BPE Dimension on Reactivity and Determination of Minimum Characteristic Dimension Required

In Figure 5(a–c), we demonstrated that by increasing the BPE width, we can enhance the reaction rate compared to the no-BPE system. A direct relationship between the polarization potential difference at the BPE, ΔV_{BPE}, and the strength of the resultant electric field arising from the potential applied between the driving electrodes, $V_{applied}$, can be represented by the following equation:

$$\Delta V_{BPE} = V_{applied} \times \frac{d}{L} \quad (3)$$

where L is the separation distance of the driving electrodes and d is the characteristic dimension of the conducting BPE (d is the width in this study).[27,28] This means the smaller the conductor (d) the larger the electric field, $\frac{V_{applied}}{L}$, required. In other words, when the applied electric field is kept constant, the polarization potential difference at the BPE, ΔV_{BPE}, increases with BPE width d, a wider BPE will have a larger polarization potential, ΔV_{BPE}.[27,31] Consequently, in Figure 5(a–c) as we increased the BPE width from 5 to 9 mm, we are increasing the polarization potential ΔV_{BPE} and we enhance the reactivity by a factor of 4 for the carbon foam system compared to the no-BPE system. The question arises: what are the dimensional limits for the BPE to drive the electrochemical reactions? As outlined in Figure 1, the redox reaction at the electrodes can be written as follows:

$$[BMIM]^+ + e^- \rightarrow [BMIM]^\bullet/[MIM]^\bullet \quad (4)$$

$$ClO_4^- \rightarrow ClO_3^- + O_{ads} + e^- \quad (5)$$

For these reactions to occur, activation barriers must be overcome, which can be determined from linear sweep voltammetry as noted in the experimental section. Figure 7

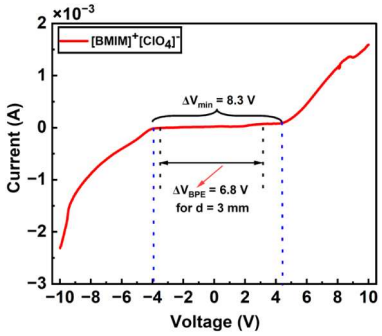

Figure 7. I–V polarization curve of $[BMIM]^+[ClO_4]^-$ by linear sweep voltammetry.

shows the I–V polarization curve for the $[BMIM]^+[ClO_4]^-$ obtained from linear sweep voltammetry. We observe that the stable potential window for this RTIL, noted as ΔV_{min} in Figure 7 is about 8.3 V, which is the minimum threshold voltage to see the onset of faradaic reactions. Additionally, for a BPE system to drive an electrochemical reaction, the potential difference at the two ends of the BPE, ΔV_{BPE}, must be higher than the stability window of the RTIL.[27] For a system, with known values of d and L, we can estimate ΔV_{BPE} from eq 3, as listed in Table 1.

Table 1. Polarization Potential According to BPE Characteristic Dimension

Characteristics BPE Dimension, d (mm)	ΔV_{BPE} (V)
9	20.5
7	16
5	11
3	6.8

We observed that the largest/widest BPE used in this study has the highest polarization potential as expected. As we decrease the BPE width to 3 mm, the calculated potential drops to a point where $\Delta V_{BPE} < \Delta V_{min}$ (Figure 7). In other words, at this dimension, the polarization potential is insufficient for the BPE to drive the redox reactions at its poles. At an applied electric field of 2.3 V/mm, the BPE needs to be at least about 3.7 mm wide to operate effectively. In other words, if the electric field remains at 2.3 V/mm, the BPE should not be narrower than 3.7 mm.

3.3. Combustion Power Generation Improvement

As outlined in Figure 1a, we have demonstrated that the apparently thermally stable, oxidation-resistant, nonvolatile, nonflammable imidazole-based RTIL, $[BMIM]^+[ClO_4]^-$ can be made flammable through electrochemical activation.[22,23] The ring structure can be broken by reduction at the cathode resulting in the gasification of combustible species. The combustion of $[BMIM]^+[ClO_4]^-$ in air under complete combustion is

https://doi.org/10.1021/acs.energyfuels.6c02293
Energy Fuels 2026, 40, 17838–17847

$$[\mathrm{BMIM}]^+[\mathrm{ClO_4}]^- + \mathrm{O_2} \rightarrow 8\mathrm{CO_2} + \frac{15}{2}\mathrm{H_2O} + \mathrm{N_2} \quad \Delta H_{(g)} = -20\ \mathrm{kJ/g} \tag{6}$$

The enthalpy of combustion used in this analysis was taken from our previous work.[23] We further extend our study to evaluate the power generation during electrochemical combustion by adopting a set of simplifying assumptions and corresponding calculations. First, under idealized conditions, we assume all the cations $[\mathrm{BMIM}]^+$ reduced at the cathode will go into the gas phase and participate in the combustion reaction. Second, we assume complete combustion. As described earlier in Section 3.1, electrochemical reactivity was quantified by measuring the current during electrolysis and relating it to current density which was further converted to surface reaction rate. If the combustion intensity can be considered proportional to the species generation rate at the surface, we can quantify the combustion power generation following the subsequent calculations. From the measured current data, we can quantify the moles of ions consumed for both BPE and no-BPE systems at specific temperatures following the equation of Faraday's law:

$$q = It \tag{7}$$

Here, I represents the measured current in amperes, and q denotes the charge consumed in coulombs. After applying the necessary unit conversions and multiplying by the combustion enthalpy, the electrochemical combustion power generation was calculated for both BPE and no-BPE systems. Figure 8 represents the combustion power generation for different BPE materials and characteristic dimensions relative to the no-BPE system. From Figure 5(a–c), it was observed that C foam has the highest species generation rate at any given BPE dimension. Consequently, the relative power generation capability of the different BPE materials for different dimensions follows the order:

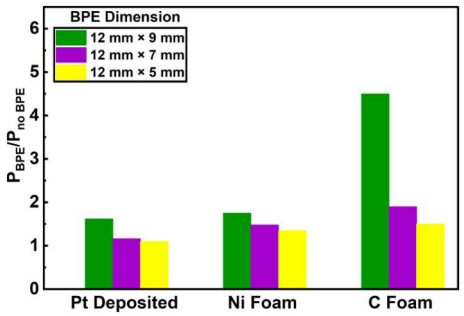

Figure 8. Electrochemical combustion power generation in BPE systems relative to no-BPE system at 25 V.

C foam > Ni foam > Deposited Pt

In practice, the values in Figure 8 should be read as theoretical upper-bound estimates rather than directly measured heat release rates. We made these estimations based on two assumptions, complete volatilization and combustion of the generated species. Regarding the assumption of complete combustion, if incomplete combustion/oxidation happens—such as CO or soot formation, or nitrogen exiting as NOx rather than N_2 would reduce the heat release relative to our calculated values. We confirmed that the electrochemically generated species transition to the gas phase and combust, we could not, however, independently quantify the volatilization yield of the RTIL investigated, which remains an unquantified source of uncertainty in the calculated absolute power values. From Figure 8 increasing the characteristic dimension of the BPEs from 5 to 9 mm improves the power generation capability by enhancing the species generation rate. Notably, the use of carbon foam with a 9 mm width can maximize power generation by a factor of ~4.5 relative to the no-BPE system. For ease of operation in a system with an 11 mm electrode separation distance, BPEs with widths up to 9 mm were used. The combustion power generation could further be enhanced by increasing the BPE width beyond this value while avoiding any short-circuiting of the cell. These results demonstrate that bipolar electrochemistry provides an effective wireless approach to boost the combustion performance of electrochemically controlled ionic liquid fuels.

3.4. Discussion on the Effectiveness of the BPE

We have experimentally demonstrated that there is substantial enhancement in electrochemical reactivity in BPE systems and argued that this might be a coupled effect of additional active surface available for faradaic reactions and potential gradient-induced improved mass transport toward the BPE poles. We also showed that there must be a minimum width of the BPE to be maintained for effective bipolar operation. To further elaborate on these points, we computed the possible potential distribution and current and reactivity enhancement in a BPE system.

The current/reactivity enhancement in the BPE system relative to that in the no-BPE system can be explained by the coexistence of two current pathways. In the no-BPE configuration, we have seen from our prior work and in this paper that the charge transfer kinetics scale with the ion conductivity of the bulk electrolyte, indicating that reactivity is limited by ion transport.[22] The introduction of a BPE conductor positioned between the driving electrodes creates an additional Faradaic current pathway that bypasses solution resistance. The reactant species are reduced at the cathodic pole of the BPE and oxidized at the anodic pole with electrons transiting through the BPE conductor to complete the circuit. This mechanism is directly evidenced by the evolution of gas bubbles observed at both tips of the BPEs during electrolysis (Figure 3).

A simple model was constructed based on our specific experimental cell geometry, assuming a linear electrical potential over the cell and a floating potential for the BPE, and run via *Claude ai*.[41]

The model assumed that ion transport to all electrode surfaces could be treated as one-dimensional migration under the applied field. The applied field of 2.3 V mm^{-1} over the cell is strong, placing it in a field-dominated transport regime. The electrolyte is assumed to follow the Vogel–Fulcher–Tammann ion-conductivity model. In this regard, there are two current contributions for the BPE system, one flowing through the BPE and one which can be considered a bypass, flowing through the area that is not blocked by the BPE between the driving electrodes. In the model we considered both nonisothermal and isothermal behavior for current/reactivity enhancement analysis.

Current/reactivity enhancement in the BPE system requires the formation of electrochemically active zones (overpotential

https://doi.org/10.1021/acs.energyfuels.6c02293
Energy Fuels 2026, 40, 17838–17847

higher than the threshold) at the BPE poles. The redox-active zone at each tip of the BPE (of width 9 mm) is computed to be 2.67 mm which occupies 59% of the total BPE width, d, with the remaining 3.65 mm forming a passive dead zone in the center where the overpotential is insufficient to sustain Faradaic reactions (Figure S1). This is consistent with our experimental finding that for effective bipolar operation, the BPE width cannot be less than 3.7 mm when the applied electric field is 2.3 V/mm. The BPE enhancement under isothermal conditions is computed to be ∼2.3× (T = ∼25 °C) and is a direct consequence of the additional Faradaic surface area presented by the BPE to migrating ions (Figure S2a−b) and is consistent with our experimentally found enhancement of ∼2× at 25 °C. In the no-BPE reference, the current is set by the bulk ohmic resistance over the full 11 mm cell gap. Inserting the BPE creates two electrochemically active zones of width, l_{act} within the bulk electrolyte and can be written in general as follows:[27,28]

$$l_{act} = (\Delta V_{BPE}/2 - V_{threshold})/E \quad (8)$$

where ΔV_{BPE} is the polarization potential difference at the BPE, $V_{threshold}$ is the onset potential of faradic reduction/oxidation of the electrolyte, and E is the applied electric field.

This active area is the additional faradic reaction surface available for the BPE case which contributes entirely and partially to the reactivity enhancement for isothermal and nonisothermal cases, respectively. The BPE operates as an internal ionic loop, where anion oxidation creates electrons which are conducted within the BPE to the cathode region of the BPE, where reduction occurs. Because the ions are "locally sourced", they are not traveling the full length of the cell. As a result, it contributes as an additional current source on top of the bypass current. As such, the practical implication is that isothermal enhancement is a purely geometric quantity and is controlled by cell dimensions, BPE dimensions, the threshold potential, and the applied potential, and is independent of temperature, ionic conductivity, and electrolyte identity. For isothermal conditions, increasing the BPE width (d) and applied potential (V) increases the polarization potential difference at the BPE, ΔV_{BPE}(eq 3). An increase in ΔV_{BPE} and a decrease in the onset threshold ($V_{threshold}$) (eq 8) result in the enhancement of the active area available for faradic reactions in the BPE system, thereby improving the overall reactivity. For demonstration purposes, in Figure S3 the effect of area enhancement on the reactivity is presented where the area is varied by changing the BPE width, (d).

One of our critical experimental findings is that our system is not necessarily isothermal for both BPE and no-BPE systems, and they heat at different rates. Since the BPE system generates greater current, it dissipates proportionally more Joule power, initiating a greater thermal response, which supplements the current generation and works like a feedback loop. The capacity of Joule heating to substantially amplify the BPE enhancement is directly tied to the nonlinear temperature dependence of $[BMIM]^+[ClO_4]^-$ conductivity, described by the Vogel−Fulcher−Tammann equation (eq 2). Under higher differential Joule heating following the VFT nonlinearity, the BPE system acquires a conductivity advantage that translates directly into current enhancement compared to the no-BPE system. The model demonstrates that the temperature difference between the two systems produces a 2.9-fold conductivity/reactivity enhancement for the BPE system that amplifies the geometric enhancement to a total of 6.9-fold at t = 60 s, of which 34% is geometric and 66% is thermal in origin (Figure S4). Experimentally, we demonstrated a 4.5-fold increase at t = 60 s for the BPE system relative to no-BPE system. So, the model can be regarded as reasonable.

These findings establish that BPE current enhancement in an ionic liquid electrolyte is a two-stage phenomenon with separable geometric and thermal contributions. The geometric stage, available immediately at the onset of the experiment, depends only on the BPE topology and cell dimensions, and the thermal stage unique to high-viscosity ionic liquids with steep VFT conductivity profiles multiplies the geometric enhancement by the corresponding conductivity enhancement. These findings have direct implications for the design of improved electrochemical combustion performance of ionic liquid fuels, where the interplay between BPE geometry, applied voltage/field, and thermally assisted ion transport determines the achievable performance enhancement.

4. CONCLUSIONS

In this study, we introduce the relatively recent concept of "bipolar electrochemistry" to enhance the kinetics of electrochemically combustible species generation in RTIL fuels. Owing to its wireless nature, this approach is particularly attractive and, to the best of our knowledge, is introduced here for the first time in the context of condensed-phase fuels. Electric field-induced polarization of a conductive bipolar electrode (BPE) immersed in the electrolyte solution enables simultaneous cathodic and anodic reactions at spatially distinct poles using a single power supply and two driving electrodes. Through electrochemical measurements, we estimated the volatile combustible gaseous species generation rates for three different materials and three different dimensions, and the results were benchmarked against a no-BPE system. Among the materials studied, carbon foam known for its high specific surface area and porosity exhibited superior performance. The incorporation of BPE enabled simultaneous faradaic reactions at the poles along with the driving electrodes resulting in up to a 4-fold enhancement in gaseous species generation rate relative to a no-BPE system. Additionally, we found the rates can be tuned further through variation of characteristic BPE dimensions. Contrary to classical isothermal reactions, where the consumption of reactants leads to a decrease in rates, we observed an increase in rates for both BPE and no-BPE systems according to the corresponding instantaneous temperature rise. Thermal imaging revealed that our systems are not isothermal and heat up at different rates driven by ionic Joule heating. Higher Joule heat-assisted temperature rise was observed for the BPE system than the no-BPE system arising from better ion transport. Normalization of reaction rates associated with BPE systems using ion transport properties such as conductivities estimated from the Vogel−Fulcher−Tammann (VFT) correlation showed temperature-independent behavior, confirming that the system remains mass transport limited despite the enhanced kinetics. Analysis of electrochemical combustion power generation demonstrated an increase for carbon foam BPE systems relative to no-BPE system by a factor of ∼4.5. Furthermore, we developed a model for predicting the reactivity enhancement and factors that influence the enhancement. We found that under isothermal conditions, the enhancement in the BPE system by a factor of ∼2.3 is purely a geometric effect and can be tuned further by adjusting the cell dimensions, BPE dimensions, threshold, and applied potential. Under non-

https://doi.org/10.1021/acs.energyfuels.6c02293
Energy Fuels 2026, 40, 17838−17847

isothermal conditions of higher differential Joule heating, the BPE system benefits from the acquired conductivity advantage which amplifies the geometric effect and gives a total enhancement by a factor of ~6.9. Overall, the experimental and computational results of this study present bipolar electrochemistry as a powerful and scalable strategy for enhancing the electrochemical combustion performance of RTIL fuels using minimal hardware, offering a promising pathway toward safer and more efficient condensed-phase energy systems.

■ ASSOCIATED CONTENT

Data Availability Statement

The data that support the findings are available upon reasonable request to the corresponding author.

Supporting Information

The Supporting Information is available free of charge at https://pubs.acs.org/doi/10.1021/acs.energyfuels.6c02293.

RTIL preparation and characterization; VFT fitting parameters; power calculation and potential distribution and reactivity enhancement in the BPE system based on the developed model (PDF)

■ AUTHOR INFORMATION

Corresponding Author

Michael R. Zachariah − *University of California, Riverside, California 92507, United States;* orcid.org/0000-0002-4115-3324; Email: mrz@engr.ucr.edu

Authors

Afrida Anis − *University of California, Riverside, California 92507, United States*

Keren Shi − *University of California, Riverside, California 92507, United States*

Erik Hagen − *University of California, Riverside, California 92507, United States*

Complete contact information is available at: https://pubs.acs.org/10.1021/acs.energyfuels.6c02293

Notes

The authors declare no competing financial interest.

■ ACKNOWLEDGMENTS

The work is supported by the US Army DEVCOM.

■ REFERENCES

(1) Spalding, D. B. Combustion of Liquid Fuels. *Nature* **1950**, *165* (4187), 160.

(2) Nakamura, M.; Akamatsu, F.; Kurose, R.; Katsuki, M. Combustion Mechanism of Liquid Fuel Spray in a Gaseous Flame. *Phys. Fluids* **2005**, *17* (12), 123301.

(3) Saldana, D. A.; Starck, L.; Mougin, P.; Rousseau, B.; Creton, B. Prediction of Flash Points for Fuel Mixtures Using Machine Learning and a Novel Equation. *Energy Fuels* **2013**, *27* (7), 3811−3820.

(4) Bier, M.; Dietrich, S. Vapour Pressure of Ionic Liquids. *Molecular Phys.* **2010**, *108* (2), 211−214.

(5) Bara, J. E.; Camper, D. E.; Gin, D. L.; Noble, R. D. Room-Temperature Ionic Liquids and Composite Materials: Platform Technologies for CO2 Capture. *Acc. Chem. Res.* **2010**, *43* (1), 152−159.

(6) Tokuda, H.; Tsuzuki, S.; Susan, A. B. H.; Hayamizu, K.; Watanabe, M. How Ionic Are Room-Temperature Ionic Liquids? An Indicator of the Physicochemical Properties. *J. Phys. Chem. B* **2006**, *110* (39), 19593−19600.

(7) Chen, C. C.; Liaw, H. J.; Chen, Y. N. Flammability Characteristics of Ionic Liquid 1-Decyl-3-Methylimidazolium Bis-(Trifluoromethylsulfonyl)Imide. *J. Loss Prev. Process Ind.* **2017**, *49*, 620−629.

(8) Sun, H.; Zhu, G.; Xu, X.; Liao, M.; Li, Y.-Y.; Angell, M.; Gu, M.; Zhu, Y.; Hung, W. H.; Li, J.; Kuang, Y.; Meng, Y.; Lin, M.-C.; Peng, H.; Dai, H. A Safe and Non-Flammable Sodium Metal Battery Based on an Ionic Liquid Electrolyte. *Nat. Commun.* **2019**, *10* (1), 3302.

(9) Aghmih, K.; Boukhriss, A.; El Bouchti, M.; Ait Chaoui, M.; Majid, S.; Gmouh, S. Introduction of Ionic Liquids as Highly Efficient Plasticizers and Flame Retardants of Cellulose Triacetate Films. *J. Polym. Environ.* **2022**, *30* (7), 2905−2918.

(10) Schiffer, Z. J.; Biswas, S.; Manthiram, K. Ammonium Formate as a Safe, Energy-Dense Electrochemical Fuel Ionic Liquid. *ACS Energy Lett.* **2022**, *7* (10), 3260−3267.

(11) Watanabe, M.; Thomas, M. L.; Zhang, S.; Ueno, K.; Yasuda, T.; Dokko, K. Application of Ionic Liquids to Energy Storage and Conversion Materials and Devices. *Chem. Rev.* **2017**, *117* (10), 7190−7239.

(12) Fox, D. M.; Gilman, J. W.; Morgan, A. B.; Shields, J. R.; Maupin, P. H.; Lyon, R. E.; De Long, H. C.; Trulove, P. C. Flammability and Thermal Analysis Characterization of Imidazolium-Based Ionic Liquids. *Ind. Eng. Chem. Res.* **2008**, *47* (16), 6327−6332.

(13) Isaac Sam, I.; Gayathri, S.; Santhosh, G.; Cyriac, J.; Reshmi, S. Exploring the Possibilities of Energetic Ionic Liquids as Non-Toxic Hypergolic Bipropellants in Liquid Rocket Engines. *J. Mol. Liq.* **2022**, *350*, 118217.

(14) Yue, G.; Hong, S.; Liu, S.-H. Process Hazard Assessment of Energetic Ionic Liquid with Kinetic Evaluation and Thermal Equilibrium. *J. Loss Prev. Process Ind.* **2023**, *81*, 104972.

(15) Zhang, Q.; Shreeve, J. M. Energetic Ionic Liquids as Explosives and Propellant Fuels: A New Journey of Ionic Liquid Chemistry. *Chem. Rev.* **2014**, *114* (20), 10527−10574.

(16) Smiglak, M.; Reichert, W. M.; Holbrey, J. D.; Wilkes, J. S.; Sun, L.; Thrasher, J. S.; Kirichenko, K.; Singh, S.; Katritzky, A. R.; Rogers, R. D. Combustible Ionic Liquids by Design: Is Laboratory Safety Another Ionic Liquid Myth? *Chem. Commun.* **2006**, *24*, 2554−2556.

(17) Liaw, H.-J.; Liou, Y.-R.; Liu, P.-H.; Chen, H.-Y.; Shu, C.-M. Increased Flammability Hazard When Ionic Liquid [C6mim][Cl] Is Exposed to High Temperatures. *J. Hazard. Mater.* **2019**, *367*, 407−417.

(18) Liaw, H.-J.; Chen, C.-C.; Chen, Y.-C.; Chen, J.-R.; Huang, S.-K.; Liu, S.-N. Relationship between Flash Point of Ionic Liquids and Their Thermal Decomposition. *Green Chem.* **2012**, *14* (7), 2001−2008.

(19) Gobin, B.; Harvey, N.; Young, G. Combustion Characteristics of Electrically Controlled Solid Propellants Using Polymer Electrolytes. *Combust. Flame* **2022**, *244*, 112291.

(20) Khoruzhii, I. V.; Klyakin, G. F.; Taranushich, V. A.; Lachin, V. I. Electrothermal Method for Controlling the Ballistic Characteristics of Energetic Condensed Systems Based on Ammonium Nitrate. *Russ. J. Appl. Chem.* **2008**, *81* (1), 61−66.

(21) Khoruzhii, I. V.; Klyakin, G. F.; Taranushich, V. A.; Lachin, V. I. A Study of the Electrothermal Method for Control over Combustion Velocity under Atmospheric Pressure of Energetic Condensed Systems Based on Ammonium Nitrate. *Russ. J. Appl. Chem.* **2007**, *80* (8), 1295−1299.

(22) Anis, A.; Shi, K.; Hagen, E.; Wang, Y.; Biswas, P.; Zachariah, M. R. Role of Anions in the Electrochemical Modulation of Flammability of Ionic Liquids. *Combust. Flame* **2025**, *275*, 113994.

(23) Biswas, P.; Wang, Y.; Hagen, E.; Zachariah, M. R. Electrochemical Modulation of the Flammability of Ionic Liquid Fuels. *J. Am. Chem. Soc.* **2023**, *145* (30), 16318−16323.

(24) Shida, N.; Zhou, Y.; Inagi, S. Bipolar Electrochemistry: A Powerful Tool for Electrifying Functional Material Synthesis. *Acc. Chem. Res.* **2019**, *52* (9), 2598−2608.

(25) Inagi, S. Fabrication of Gradient Polymer Surfaces Using Bipolar Electrochemistry. *Polym. J.* **2016**, *48* (1), 39−44.
(26) Chow, K.-F.; Mavré, F.; Crooks, R. M. Wireless Electrochemical DNA Microarray Sensor. *J. Am. Chem. Soc.* **2008**, *130* (24), 7544−7545.
(27) Loget, G.; Zigah, D.; Bouffier, L.; Sojic, N.; Kuhn, A. Bipolar Electrochemistry: From Materials Science to Motion and Beyond. *Acc. Chem. Res.* **2013**, *46* (11), 2513−2523.
(28) Duval, J. F. L.; Buffle, J.; van Leeuwen, H. P. Quasi-Reversible Faradaic Depolarization Processes in the Electrokinetics of the Metal/Solution Interface. *J. Phys. Chem. B* **2006**, *110* (12), 6081−6094.
(29) Mavré, F.; Anand, R. K.; Laws, D. R.; Chow, K.-F.; Chang, B.-Y.; Crooks, J. A.; Crooks, R. M. Bipolar Electrodes: A Useful Tool for Concentration, Separation, and Detection of Analytes in Microelectrochemical Systems. *Anal. Chem.* **2010**, *82* (21), 8766−8774.
(30) Perdue, R. K.; Laws, D. R.; Hlushkou, D.; Tallarek, U.; Crooks, R. M. Bipolar Electrode Focusing: The Effect of Current and Electric Field on Concentration Enrichment. *Anal. Chem.* **2009**, *81* (24), 10149−10155.
(31) Wang, Y.-L.; Cao, J.-T.; Liu, Y.-M. Bipolar Electrochemistry − A Powerful Tool for Micro/Nano-Electrochemistry. *ChemistryOpen* **2022**, *11* (12), No. e202200163.
(32) Tao, X.; Chen, X.; Xia, Y.; Huang, H.; Gan, Y.; Wu, R.; Chen, F.; Zhang, W. Highly Mesoporous Carbon Foams Synthesized by a Facile, Cost-Effective and Template-Free Pechini Method for Advanced Lithium−Sulfur Batteries. *J. Mater. Chem. A* **2013**, *1* (10), 3295−3301.
(33) Zhang, J.; Li, W.; Ahmed Shifa, T.; Sun, J.; Jia, C.; Zhao, Y.; Cui, Y. Hierarchical Porous Carbon Foam Supported on Carbon Cloth as High-Performance Anodes for Aqueous Supercapacitors. *J. Power Sources* **2019**, *439*, 227066.
(34) Mao, X.; Li, Y.; Li, Y.; Zhu, D.; Yu, W.; Ji, Y.; Wang, D.; Hu, X. Simultaneous Electrical and Mechanical Properties Improvement for Composite Expanded Graphite Bipolar Plate by Incorporating Surface-Activated Carbon Black Paving on the Carbonized Melamine Foam Skeleton. *Compos. Sci. Technol.* **2024**, *257*, 110822.
(35) Bard, A. J.; Faulkner, L. R. *Electrochemical Methods: fundamentals and Applications*; John Wiley & Sons, Inc, 2001.
(36) O'M Bockris, J.; Reddy, A. K. N. *Modern Electrochemistry 1 Ionics*; 2nd ed., Kluwer Academic; 2002, Vol. *1*.
(37) Walsh, F. C. The Kinetics of Electrode Reactions: Part I—General Considerations and Electron Transfer Control. *Trans. IMF* **1992**, *70* (1), 50−54.
(38) Karimian, N.; Hashemi, P.; Afkhami, A.; Bagheri, H. The Principles of Bipolar Electrochemistry and Its Electroanalysis Applications. *Curr. Opin. Electrochem.* **2019**, *17*, 30−37.
(39) Dojčinović, M. P.; Stojković Simatović, I.; Nikolić, M. V. Supercapacitor Electrodes: Is Nickel Foam the Right Substrate for Active Materials? *Materials* **2024**, *17* (6), 1292.
(40) Collins, G.; Barwa, T. N.; Glennon, L.; Kasturi, P. R.; Breslin, C. B. Corrosion of Nickel Foam Electrodes during Hydrothermal Reactions: The Influence of a Simple Protective Carbon Black Coating. *Electrochem. Commun.* **2024**, *169*, 107835.
(41) Anthropic *Claude (Claude Sonnet 4.6) [Large language model]* https://claude.ai.

https://doi.org/10.1021/acs.energyfuels.6c02293
Energy Fuels 2026, 40, 17838−17847